Rayleigh and leaky surface acoustic waves in proton-exchanged lithium niobate

R. Rimeika, D. Čiplys

Vilnius University, Department of Radiophysics
Physics Faculty, Saulėtekio 9, 2040 Vilnius, LITHUANIA
E-mail: daumantas.ciplys@ff.vu.lt

Introduction

The proton-exchange (PE) technique [1] is a relatively simple method for fabricating integrated optical waveguides on lithium niobate crystals. Due to strong piezoelectricity, lithium niobate is widely used in surface acoustic wave (SAW) applications [2]. An interaction between guided optical waves and SAWs in PE $LiNbO_3$ attracted much interest and has been extensively studied (see e.g. [3]). An acoustooptic frequency shifter driven by a SAW in a PE $LiNbO_3$ waveguide with a great application potential has been recently proposed [4]. It is known that the proton exchange affects SAW propagation properties, such as velocity [5] and electromechanical coupling coefficient [6]. Up to now, the SAW propagation studies in PE $LiNbO_3$ were limited by the Rayleigh-type waves. There is also much interest in studies and applications of other surface acoustic wave types, in particular, of the leaky surface acoustic waves (LSAWs) [7]). Higher velocities of LSAW as compared to the Rayleigh-wave velocities allow to achieve higher operation frequencies with the same photolithography-defined transducer dimensions. Moreover, the leaky waves on Z-cut lithium niobate are dominantly polarized in the propagation plane and hence are suitable for liquid phase sensing. It was the purpose of this work to study the propagation properties of leaky surface acoustic waves in proton-exchanged lithium niobate and compare them with Rayleigh-wave properties. We report on the results of SAW velocity and electromechanical coupling coefficient measurements performed in Z-cut X-propagation $LiNbO_3$ samples with PE layers of various thicknesses.

Transducer impedance measurements

PE waveguides have been fabricated in optical-grade Z-cut lithium niobate substrates. $H_xLi_{1-x}NbO_3$ layers of various thicknesses and molar amounts of hydrogen x have been fabricated by immersing $LiNbO_3$ plates into benzoic acid, ammonium dihydrophosphate or the solution of $KHSO_4$ in glycerin, and by post-exchange annealing in air. A more detailed description of the PE process and resulting properties of $H_xLi_{1-x}NbO_3$ layers can be found elsewhere [8,9]. The $H_xLi_{1-x}NbO_3$ layer thicknesses of the samples used in our experiments are listed in Table 1. The samples S1, S2, S3, and S5 were subjected to the proton exchange only, and the sample S4 was annealed after the exchange procedure. An interdigital transducer (IDT) for SAW excitation has been deposited on a sample surface, and the frequency dependence of the IDT input impedance, $Z(f)$, has been measured with the network analyzer. The transducer periods and hence the acoustic wavelengths were 24, 40, and 50 μm. The SAW propagation direction was along the X-axis of $LiNbO_3$. For each sample, measurements on a non-exchanged part of the surface could be performed for reference. An example of measured real part of the transducer impedance is shown in Fig. 1.

Table 1.

Sample	S1	S3	S2	S5	S4
d (μm)	1.85	2.14	2.85	4.3	9.15

The observed two maxima in the Re$Z(f)$ dependence can be attributed to the Rayleigh (lower frequencies) and leaky surface acoustic waves, respectively (see, e.g. [10]).

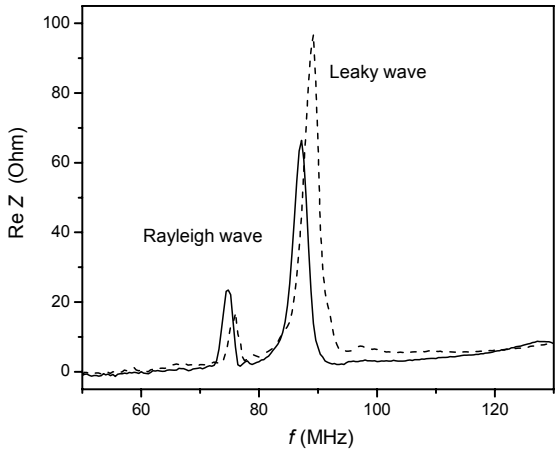

Fig. 1 **Frequency dependence of the real part of transducer impedance. Sample S1, acoustic wavelength Λ =50 μm. Dashed line: non-exchanged surface; solid line: proton-exchanged surface**

One can see that the proton exchange affects the peak position in the frequency scale as well the peak height. This implies that the proton exchange leads to the changes in SAW velocity and the electromechanical coupling coefficient both for the Rayleigh and leaky waves. These changes can be extracted from the quantitative analysis of the transducer impedance.

Evaluation of transducer properties

The equivalent circuit of the interdigital transducer deposited on a piezoelectric substrate is shown in Fig. 2, where G_a and B_a stand for the real and imaginary parts of the radiation admittance, respectively, C_T is the static

capacitance of the IDT, C_p and L_p are the stray capacitance and inductance, respectively.

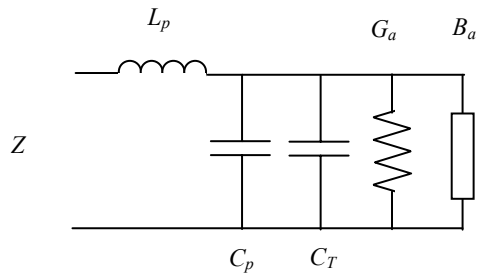

Fig. 2. **Equivalent circuit of the SAW transducer**

The dependencies of G_a and B_a on the frequency f are given [11] by:

$$G_a = 8K^2 f_0 C_T N \left(\frac{\sin X}{X}\right)^2, \quad (1)$$

$$B_a = 8K^2 f_0 C_T N \frac{\sin 2X - 2X}{2X^2}, \quad (2)$$

where

$$X = N\pi(f - f_0)/f_0, \quad (3)$$

$$f_0 = V/\Lambda, \quad (4)$$

K^2 is the electromechanical coupling coefficient, f_0 is the transducer center frequency, V is the SAW velocity, Λ is the acoustic wavelength, and N is the number of transducer periods. The real and imaginary parts of IDT input impedance Z can be respectively expressed as:

$$\mathrm{Re}\, Z = \frac{G_a}{G_a^2 + B^2}, \quad (5)$$

$$\mathrm{Im}\, Z = 2\pi f L_p - \frac{B}{G_a^2 + B^2}, \quad (6)$$

where

$$B = B_a + 2\pi f C, \quad (7)$$

and

$$C = C_T + C_p. \quad (8)$$

The intrinsic capacitance of the overlapping transducer fingers is

$$C_T = C_0 NL, \quad (9)$$

where L is the finger overlap length (IDT aperture), and C_0 is the capacitance per IDT period and per unit finger length. Values of C_0 have been reported in literature for various materials. For example, C_0=0.46 pF/mm for YZ $LiNbO_3$ [2]. For the layer-on-substrate structure, the capacitance C_0 can be calculated from the expression [12]:

$$C_0 = 9.06\left(\varepsilon_f + 1 + (\varepsilon_s - \varepsilon_f)\exp(-9.2d/\Lambda)\right), \quad (10)$$

where ε_0 is the free-space dielectric constant, ε_f and ε_s are the relative dielectric constants of a layer and a substrate, respectively, and d is the layer thickness. Using the capacitance meter in the kilohertz range, we have measured the capacitances of various transducers deposited on our samples and plotted them as a function of period number-aperture product NL as shown in Fig. 3. The measured values are in a good agreement with the linear dependence of Eq. 10 with the slope C_0=0.46 pF/mm. Hence, we conclude that the stray capacitance C_p is negligible, and the net capacitance C_T is determined in these measurements. Typically, we observed a slight increase in the IDT capacitance after the proton exchange, in accordance with the enhancement of the dielectric constant in an $H_xLi_{1-x}NbO_3$ layer, but this increase was not important in our studies.

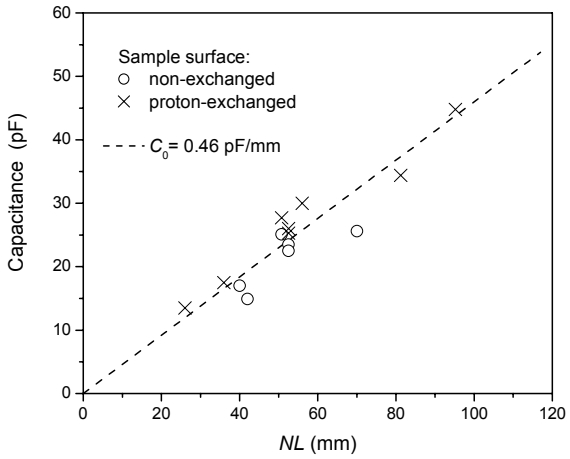

Fig. 3. **Measured transducer capacitances versus period number-aperture product. Dashed line shows the slope for YZ $LiNbO_3$ [2].**

The sample fixture used in the network analyzer measurements had a larger stray capacitance C_p, which could not be neglected. Also, at the frequencies of the order of a hundred megahertz, the stray inductance L_p should be accounted for. At frequencies far away from the center frequency f_0, $G_a = B_a = 0$, and

$$\mathrm{Im}\, Z = 2\pi f L_p - \frac{1}{2\pi f C}. \quad (11)$$

The total capacitance C=C_T+Cp and inductance L_p were found by fitting, in a wide frequency range, the calculated and measured $\mathrm{Im}\, Z(f)$ dependencies as shown in Fig. 4. Typically, the difference between C and C_T was 2 to 4 pF.

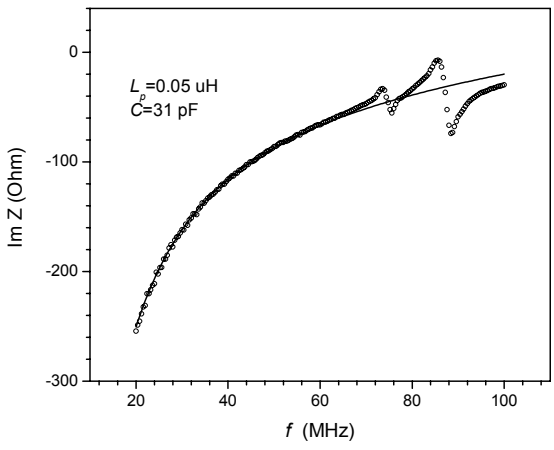

Fig. 4 **Frequency dependence of the imaginary part of the transducer impedance. Dots, as measured; solid line, calculated from Eq. 11 with C and L_p as fitting parameters. Sample S1, PE surface**.

Extraction of SAW velocity and electromechanical coupling coefficient

From Eq. 5 and 6 we calculated the frequency dependencies of real and imaginary parts of the IDT impedance and fitted them to the experimentally measured ones, using the SAW velocity V and electromechanical coupling coefficient K^2 as fitting parameters. The values of C, C_T and L_p, determined as described above were used in calculations. The fitting curves for Rayleigh waves on protonated and non-protonated surface of the sample S1 are shown in Fig. 5 and 6, and those for leaky waves are shown in Fig. 5 and 6.

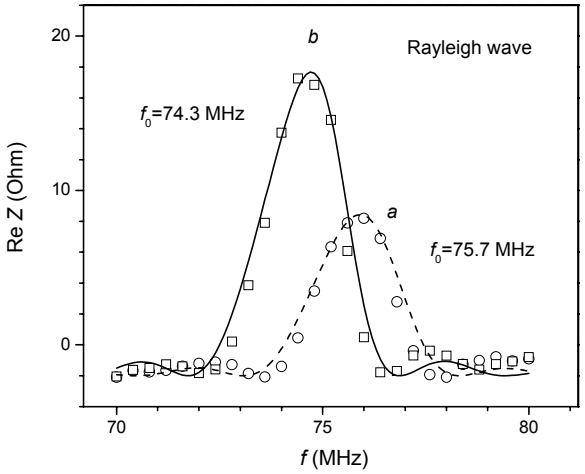

Fig. 5. **Real part of IDT impedance for Rayleigh waves. Sample S1 with PE layer thickness d=1.85 μm. Dots, experiment. Lines, theory with fitting parameters: a) non-exchanged surface, V=3785 m/s, K^2 =0.45 %; b) proton-exchanged surface, V =3715 m/s, K^2 =0.85 %. The center frequencies f_0 are indicated at the corresponding curves**.

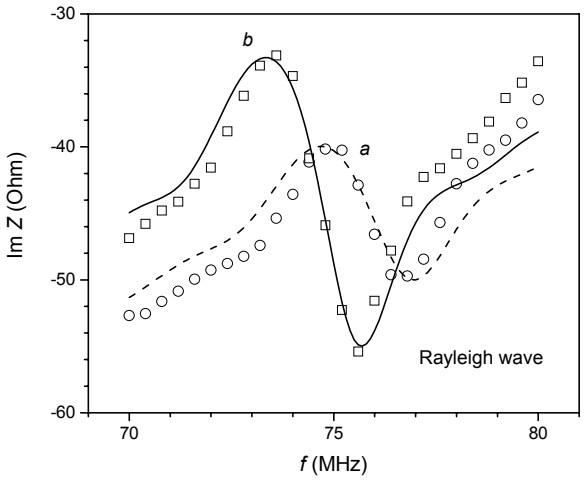

Fig. 6. **Imaginary part of IDT impedance for Rayleigh waves in sample S1. Dots, experiment. Lines, theory with the same fitting parameters as in Fig. 5; a) non-exchanged surface, b) proton-exchanged surface**

On the surface not subjected to the proton exchange, the velocity and the electromechanical coupling coefficient of the leaky wave are higher than the corresponding parameters of the Rayleigh wave, in accordance with what has been observed previously [10]. The proton exchange leads to significant changes both in the SAW velocity and electromechanical coupling coefficient values.

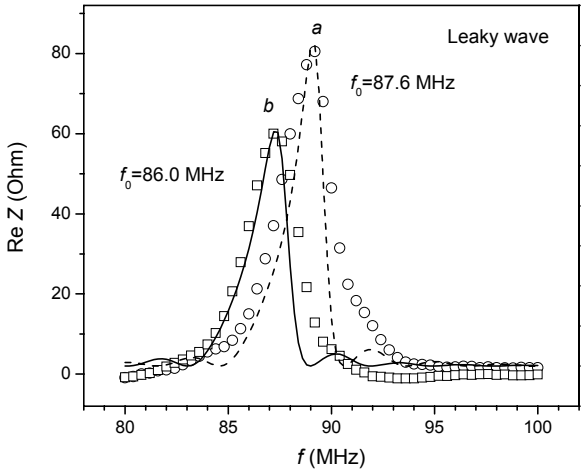

Fig. 7. **Real part of IDT impedance for leaky waves. Sample S1. Dots, experiment. Lines, theory with fitting parameters: a) non-exchanged surface, V=4380 m/s, K^2 =3.1 %; b) proton-exchanged surface, V =4300 m/s, K^2 =2.5 %. The center frequencies f_0 are indicated at the corresponding curves**

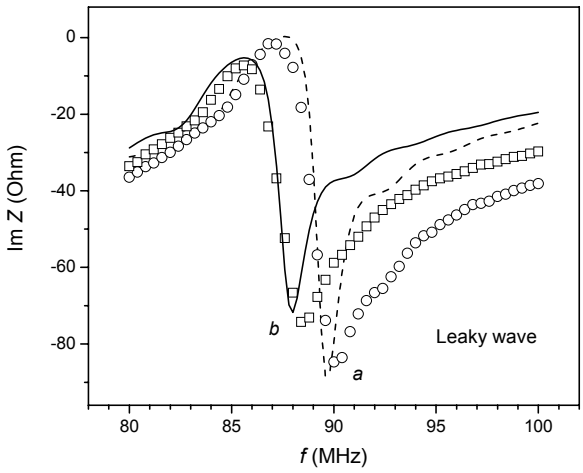

Fig. 8. **Imaginary part of IDT impedance for leaky waves in sample S1. Dots, experiment. Lines, theory with the same fitting parameters as in Fig. 7; a) non-exchanged surface, b) proton-exchanged surface**

The extracted values of the SAW velocity and the electromechanical coupling coefficient are plotted in Fig. 9 and 10 both for leaky and Rayleigh waves as a function of acoustic wave number-protonated layer thickness product, kd, where $k = 2\pi/\Lambda$. In agreement with the earlier observations [9], the Rayleigh wave velocity exhibits a linear decrease with kd. We observe that the proton exchange leads to the leaky wave velocity decrease in a similar way, with a slope very close to that of the Rayleigh wave. For both types of the SAW, the post-exchange annealing of the sample led to the partial restitution of the SAW velocity towards the initial value.

As one can see from Fig. 10, the electromechanical coupling coefficient for Rayleigh waves in ZX-$LiNbO_3$ can be increased by the proton exchange. This observation confirms the result we have previously obtained using a different method for K^2 evaluation [6]. For the leaky waves,

we observe that the proton exchange considerably reduces the electromechanical coupling coefficient. It should be noted that the K^2 values for leaky waves are rather scattered, even for the non-exchanged surface. Nevertheless, the K^2 drop is evident at kd >0.4.

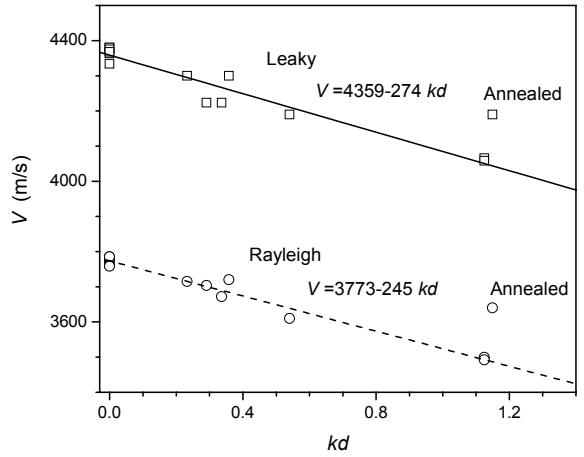

Fig. 9. **Leaky and Rayleigh SAW velocities in proton-exchanged ZX $LiNbO_3$ as functions of wave number-layer thickness product *kd* . Dots, experiment; lines, linear approximations with slopes indicated. The *V* values obtained in a post-annealed sample are also shown**

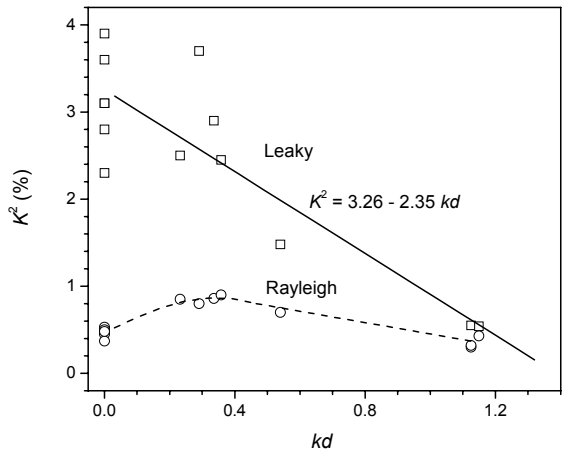

Fig. 10. **Electromechanical coupling coefficients for leaky and Rayleigh SAW velocities in proton-exchanged ZX $LiNbO_3$ as functions of layer-layer thickness product *kd* . Dots, experiment; solid line for leaky wave, linear approximation; dashed line for the Rayleigh wave, guide for an eye.**

Conclusions

We have studied the properties of leaky surface acoustic waves propagating along X-axis on Z-surface of proton-exchanged lithium niobate and compared them to the properties of Rayleigh-type SAWs. From the interdigital transducer impedance measurements, the SAW velocities and the electromechanical coupling coefficients have been extracted in a wide range of acoustic wave number- protonated layer thickness product *kd* values. Our study revealed that the proton exchange led to the slight linear decrease of the leaky wave velocity with growing *kd* in a similar way as in the case of the Rayleigh waves. A considerable reduction of the electromechanical coupling coefficient has been observed for the leaky waves in the proton-exchanged samples with *kd* values of the order of unity, in contrast with steady and even slightly enhanced values of K^2 for Rayleigh waves.

References

1. **Jackel J. L., Rice C. E., and Veselka J. J**. Proton exchange for high-index waveguides in $LiNbO_3$. Appl. Phys. Lett. 1982. Vol. 41. P. 607-608.
2. **Campbell C. K**. Surface acoustic wave devices for mobile and wireless communications. Academic press, Boston. 1998.
3. **Rimeika R., Ciplys D. and Balakauskas S**. Diffraction of guided optical waves by surface acoustic waves in proton-exchanged 128° rotated Y-cut $LiNbO_3$ Phys. Stat. Sol. (a). 2001. Vol. 184. P. 217-223.
4. **Kakio S., Kitamura M., Nakagawa Y., Zou N., Hara T., Ito H., Iizuka T., Kobayashi T., Watanabe M**. Waveguide- type acoustooptic frequency shifter driven by surface acoustic wave and its application to frequency-shifted feedback fiber laser. IEEE Ultrasonics Symposium Proc. 2003. P. 1808-1811.
5. **Hinkov V. and Ise B**. Surface acoustic velocity perturbation in $LiNbO_3$ by proton exchange. J. Phys. D: Appl. Phys. 1985. Vol. 18. P. L31-L34.
6. **Čiplys D., Rimeika R., Korkishko Yu. V., Fedorov V.A.** Enhancement of electromechanical coupling coefficient by proton exchange in Z-cut $LiNbO_3$ Appl. Phys. Lett. 2000. Vol. 76. P. 433-435.
7. **Takayanagi A., Yamanouchi K. and Shibayama K**. Piezoelectric leaky surface wave in $LiNbO_3$. Appl. Phys. Lett. 1970. Vol. 17. P.225-227.
8. **Korkishko Yu. N., Fedorov V. A**. Structural phase diagram of $H_xLi_{1-x}NbO_3$ waveguides: the correlation between optical and structural properties. IEEE J. Sel. Topics Quantum Electron. 1996. Vol. 2. P.187-196.
9. **Fedorov V. A., Korkishko Yu. N., Ciplys D. and Rimeika R**. Velocity of SAWs in proton-exchanged waveguides in $LiNbO_3$. Properties of Lithium Niobate - EMIS Data Review Series. Ed. Wong, K.K. INSPEC-IEE, London. 2002. P. 254-262.
10. **Bu G., Čiplys D., Shur M. S., Namkoong G., Doolittle W. and Hunt W. D**. Leaky surface acoustic waves in Z-$LiNbO_3$ substrates with epitaxial AlN overlays. Appl. Phys. Lett. 2004. Vol. 85. P. 3313-3315.
11. **Smith W.R., Gerard H. M., Collins J. H., Reeder T. M. and Shaw H. J**. Analysis of interdigital surface wave transducers by use of an equivalent circuit model. IEEE Trans. Microwave Technology and Techniques. 1969. Vol. MTT-17. P. 856-864.
12. **Al-Shareef H. N., Dimos D., Raymond M. V., Schwartz R. W. and Mueller C. H**. Tunability and calculation of the dielectric constant of capacitor structures with interdigital electrodes. J. of Electroceramics. 1997. Vol. 1. P. 145-153.

R. Rimeika, D. Čiplys

Paviršinės akustinės nuotėkio bangos protonuotame z-pjūvio ličio niobate

Reziumė

Protonų mainų technologija yra veiksmingas būdas optiniams šviesolaidžiams piezoelektriniuose ličio niobato kristaluose sudaryti. Paviršinių akustinių bangų ir šviesolaidžio modų sąveika įgalina sukurti įvairius akustooptinius šviesos valdymo įtaisus, todėl svarbu ištirti paviršinių akustinių bangų sklidimo protonuotame ličio niobate charakteristikas. Iki šiol palyginti neblogai buvo ištirtos *Rayleigh* bangos, sklindančios įvairiai orientuotuose PE $LiNbO_3$ kristaluose. Z-pjūvio ličio niobate gali sklįsti ir kitos - nuotėkio paviršinės akustinės - bangos. Ištirti protonų mainų įtaką jų savybėms ir buvo šio darbo tikslas. Vektorinių grandinių analizatoriumi matavome PAB keitiklio impedansą. Lygindami eksperimentines impedanso priklausomybes su teorinėmis, nustatėme akustinių bangų greičius ir elektromechaninio ryšio koeficientus. Z-pjūvio ličio niobate protonų mainai mažina tiek nuotėkio, tiek *Rayleigh* bangų greitį, o jų santykis išlieka maždaug pastovus. Gryname ZX ličio niobate nuotėkio bangų elektromechaninio ryšio koeficientas yra kur kas didesnis už *Rayleigh* bangų koeficientą. Didėjant protonuoto sluoksnio storiui (arba PAB dažniui), *Rayleigh* bangų K^2 pasiekia maksimumą, o nuotėkio bangų - monotoniškai mažėja.

Pateikta spaudai 2005 06 27